J Mater Sci (2012) 47:883–891
DOI 10.1007/s10853-011-5868-y

A neural network approach for the prediction of the refractive index based on experimental data

Alex Alexandridis · Eva Chondrodima · Konstantinos Moutzouris · Dimos Triantis

Received: 26 May 2011 / Accepted: 10 August 2011 / Published online: 24 August 2011

Abstract This article presents a systematic approach for correlating the refractive index of different material kinds and forms with experimentally measured inputs like wavelength, temperature, and concentration. The correlation is accomplished using neural network models, which can deal effectively with the nonlinear nature of the problem without requiring a predefined form of equation, while taking into account all the parameters affecting the refractive index. The proposed methodology employs the powerful radial basis function network architecture and the neural network training procedure is accomplished using an innovative algorithm, which provides results with increased prediction accuracy. The methodology is applied to two cases, involving the estimation of the refractive index of semiconductor material crystals and an ethanol–water mixture and the results show that the refractive index predictions are accurate approximately to the same number of decimal places as the real measurements. Comparisons with other neural network training methods, but also with empirical forms like the Sellmeier equation, highlight the superiority of the proposed approach.

Introduction

The refractive index n of a material is expressed as the ratio of the velocity of light in vacuum relative to the velocity of light in the considered material. The refractive index is a fundamental physical property of substance related not only to its optical, but also electrical, magnetic, thermal, and mechanical properties [1–4]. In general, n depends on light wavelength and temperature, effects commonly referred to as chromatic and temperature dispersion, respectively. However, in many situations there exist numerous additional parameters influencing the refractive index, ranging from doping level and composition in amorphous materials and semiconductor or dielectric crystals [5–9], to particle size and concentration in nanocomposite materials [10–12], salinity and pressure in seawater [13, 14], humidity and CO_2 content in air [15], etc.

Several instruments (often commercially available) are employed for the experimental measurement of the refractive index, exploiting interferometric [16], deviation [17], critical angle [18], Brewster angle [19], index matching [20], and immersion [21] approaches. Most typically, the achievable accuracy with these standard setups is approximately equal to, or just exceeds, four decimal digits. However, recent advances in laser technology seem to pave the way for significant improvements in this field; for instance, the refractive index of several gases has been determined with a precision reaching nine decimal digits by use of a relatively expensive and complicated frequency comb setup [22].

The development of ultra-precise refractive index measurement techniques that detect more than four decimal digits may be useful for several nanophotonics engineering applications. For example, the calculation of grating period Λ for quasi-phase-matching nonlinear interactions requires knowledge of the refractive index at the interacting wavelengths [23]. Previous material processing obstacles that limited grating period Λ to the micrometer scale now seem to be raised, permitting for the first time the fabrication of quasi-phase-matching nanostructures [24]. This

A. Alexandridis (✉) · E. Chondrodima · K. Moutzouris · D. Triantis
Laboratory of Electric Properties of Materials, Department of Electronics, Technological Educational Institute of Athens, Agiou Spiridonos, 12210 Aigaleo, Greece
e-mail: alexx@teiath.gr

size reduction naturally generates the need for even more accurate knowledge of n. Other applications with similarly stringent requirements include optical metrology [25], as well as various optical diagnostic systems for the identification of a particular substance [26], the confirmation of its purity [27], or the measurement of its concentration [28].

In such situations, precise measurement of the refractive index is not sufficient in itself, due to the fact that experimental data are available only at discrete experimental conditions. In order to predict n outside measurement conditions, numerous empirical or semi-empirical modeling solutions have been proposed. Building such models is not an easy task, since the relationship between the refractive index and the parameters affecting it is usually nonlinear in nature and quite often poorly understood. In the simplest case only wavelength dependence is considered to produce chromatic dispersion relations of the Sellmeier form [29]. Temperature dependence may also be accounted for by use of an extended temperature-dependent Sellmeier-type equation [30]. Several studies have reported the inclusion of additional parameters in specific situations. Indicatively, Liu and Daum [31] investigated the consistency of mixing rules for calculating the effective refractive index for multicomponent mixtures. Xu et al. [32] built a quantitative structure–property relationship model to predict n for linear polymers by applying four molecular descriptors. Rabah et al. [33] calculated the refractive index—among other properties—of binary semiconductor compounds based on empirical methods. Yu et al. [34] used density functional theory (DFT) calculations for the prediction of the refractive index of vinyl polymers. Cao et al. [35] employed the Eisenlohr and Vogel methods to estimate the refractive index for pharmaceutical solids.

Evidently, the development of ultra-precise refractive index measurement techniques should be followed by the development of novel, more powerful simulation tools. In this study, we present the use of neural networks [36] for predicting the refractive index of various material forms (crystals and binary mixtures) using as inputs experimental data. In order to achieve better accuracy, we are employing a special architecture called radial basis function (RBF) networks [37], using a non-symmetric version of the fuzzy means algorithm [38] as training technique. Having the ability to identify underlying highly complex and nonlinear relationships from input–output data only, the neural network approach presents certain advantages: (a) it is applicable to any material or material form, (b) it can account for all parameters affecting n, without requiring a predefined form of equation, and (c) it offers increased precision in the refractive index prediction.

Not surprisingly, the capabilities of neural networks have already been exploited for modeling and simulation in materials science: Ning [39] has correlated the glass transition temperature of fluorine-containing polymers with three structural parameters using neural networks. Important work has also been done in applying neural networks for predicting critical parameters in steel materials [40–43]. Other computational intelligence methodologies like fuzzy logic [44] and genetic algorithms [45–47] have also been applied successfully. As far as specific applications of neural networks for refractive index model building are concerned, Ghosh et al. [48] modeled a plasma-enhanced chemical vapor deposition (PECVD) process and predicted the refractive index and the deposition rate of PECVD silicon nitride films using neural networks. Tabet and McGahan [49] used neural networks to calculate the thickness and refractive index of thin films from spectroscopic reflectometry data. However, these approaches use as inputs process-specific parameters, contrary to the methodology proposed in this article which is completely application-independent.

The rest of this article is organized as follows: In the next section, we present the RBF neural network architecture, the fuzzy means training algorithm and the non-symmetric variation. In "Results and discussion", the proposed methodology is applied to two case studies. The first one concerns the prediction of the refractive index of semiconductor crystals, while the second one the prediction of the refractive index of binary mixtures. The article concludes by outlining the advantages of the proposed approach.

The RBF neural network architecture

An RBF network can be considered as a special three layer neural network, which is linear with respect to the output parameters after fixing all the RBF centers and nonlinearities in the hidden layer. The typical structure of an RBF network is shown in Fig. 1. The input layer distributes the N input variables to the L nodes of the hidden layer. Each node in the hidden layer is associated with a center, equal in dimension with the number of input variables. Thus, the hidden layer performs a nonlinear transformation and maps the input space onto a new higher dimensional space. The activity $v_l(\mathbf{x}_k)$ of the lth node is the Euclidean norm of the difference between the kth input vector and the node center and is given by:

$$v_l(\mathbf{x}_k) = \|\mathbf{x}_k - \hat{\mathbf{x}}_l\| = \sqrt{\sum_{i=1}^{N} (x_{k,i} - \hat{x}_{l,i})^2}, \quad k = 1, 2, \ldots, K \tag{1}$$

where K is the total number of data, $\mathbf{x}_k^{\mathrm{T}} = [x_{k,1}, x_{k,2}, \ldots, x_{k,N}]$ is the input vector, and $\hat{\mathbf{x}}_l^{\mathrm{T}} = [\hat{x}_{l,1}, \hat{x}_{l,2}, \ldots, \hat{x}_{l,N}]$ is the center of the lth node.

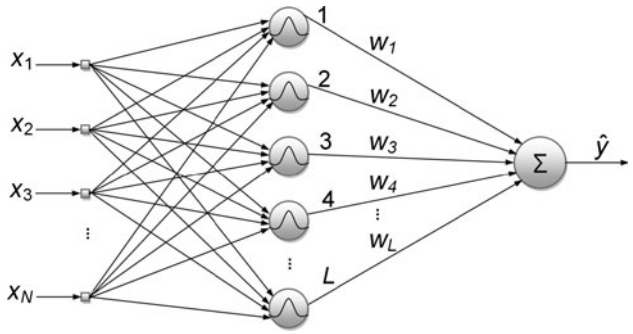

Fig. 1 Radial basis function network architecture

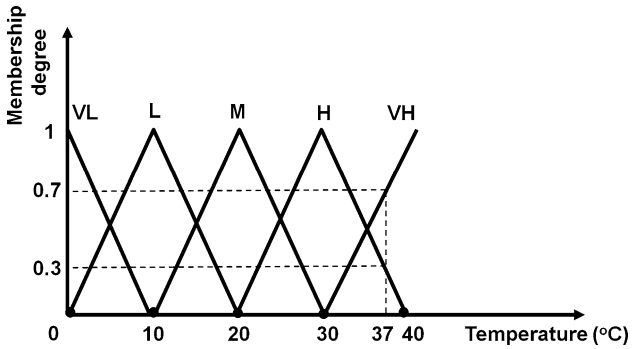

Fig. 2 Fuzzification example: conversion of a crisp temperature value to membership degrees

The output function of the node is a radially symmetric function. A typical choice, which was also used in this study, is the Gaussian function:

$$f(v) = \exp\left(-\frac{v^2}{\sigma^2}\right) \tag{2}$$

where σ is the width of the node.

The final output $\hat{y}_k$ of the RBF network for the kth data point is produced by a linear combination of the hidden node responses, after adjusting the weights of the network appropriately:

$$\hat{y}_k = \sum_{l=1}^{L} w_l f(v_l(\mathbf{x}_k)), \quad k = 1, 2, \ldots, K \tag{3}$$

where w_l stands for the synaptic weight of the lth node.

Standard approaches decompose the problem of RBF network training in two steps: The first step aims at determining the centers $\hat{\mathbf{x}}_l$ of the hidden layer nodes. A standard technique for accomplishing this task is the k-means algorithm [50], which is an unsupervised clustering method. The second step involves the determination of the output-layer weights by linear least squares regression. Recently, an innovative approach called the fuzzy means algorithm has been introduced to replace the k-means algorithm in the selection of the hidden layer nodes [38]. The fuzzy means algorithm has several advantages over the typical approach, including faster computational times and automatic determination of the size of the network, and has been used successfully in a number of applications including estimation of critical properties of materials [51, 52], online system identification [53], automatic control of industrial processes [54], variable selection problems [55, 56], etc. In this study, we are employing a non-symmetric version of the fuzzy means algorithm that provides improved results in terms of increased prediction accuracy [57]. A brief discussion about fuzzy logic, the fuzzy means algorithm, and its non-symmetric variation is given below, while the interested reader is referred to the original publications.

Fuzzy logic and the fuzzy means algorithm

The fundamental difference of fuzzy logic compared to conventional techniques is on the definition of sets [58]. Traditional set theory is based on bivalent logic where a number or object is either a member of a set or it is not. Contrary to that, fuzzy logic allows a number or object to be a member of a set to a certain degree. This degree is a number between zero and one and is called "membership degree". The function mapping the input space to membership values (or degrees) is called the membership function. One of the simplest membership functions has triangular form, where the triangle's tip defines the maximum degree of membership. The fuzzy sets defined by such membership functions are called triangular fuzzy sets. An example is given in Fig. 2, where we consider the fuzzification of a crisp temperature value. The input space in this case is partitioned to five triangular fuzzy sets named VL (Very Low), L (Low), M (Medium), H (High), and VH (Very High). A crisp temperature of 37 °C is transformed to a membership degree of 0.7 to the fuzzy set "High" and 0.3 to the fuzzy set "Very High".

Consider a system with N normalized input variables x_i, where $i = 1,\ldots,N$. The domain of each input variable is partitioned into an equal number of one-dimensional triangular fuzzy sets, c. Each fuzzy set can be written as:

$$A_{i,j} = \{a_{i,j}, \delta\alpha\}, \quad i = 1, \ldots, N, \quad j = 1, \ldots, c. \tag{4}$$

where $a_{i,j}$ is the center element of fuzzy set $A_{i,j}$, and $\delta\alpha$ is half of the respective width (due to the symmetric partition all the widths are equal). This partitioning technique creates a total of c^N multi-dimensional fuzzy subspaces $\mathbf{A}^l$, where $l = 1,\ldots,c^N$. Each multi-dimensional fuzzy subspace is generated by combining N one-dimensional fuzzy sets, one for each input direction. One can define the center vector $\mathbf{a}^l$ and the side vector $\boldsymbol{\delta\alpha}$ of each fuzzy subspace:

$$\mathbf{A}^l = \{\mathbf{a}^l, \boldsymbol{\delta\alpha}\} = \left\{ \left[a^l_{1,j_1}, a^l_{2,j_2}, \ldots, a^l_{N,j_N}\right], \left[\underbrace{\delta\alpha, \delta\alpha, \ldots, \delta\alpha}_{N}\right] \right\}, \quad l = 1, \ldots, c^N \tag{5}$$

where a^l_{i,j_i} is the center element of the one-dimensional fuzzy set A_{i,j_i} that has been assigned to input i. Each one of the produced fuzzy subspaces is a candidate for becoming an RBF center, but only a few of those will be finally selected. The selection is based on the idea of the multidimensional membership function $\mu_{\mathbf{A}^l}(\mathbf{x}_k)$ of an input vector $\mathbf{x}_k$ to a fuzzy subspace $\mathbf{A}^l$ which is given by Nie [59]:

$$\mu_{A^l}(\mathbf{x}_k) = \begin{cases} 1 - r_l(\mathbf{x}_k), & \text{if } r_l(\mathbf{x}_k) \le 1 \\ 0, & \text{otherwise} \end{cases} \tag{6}$$

where $r_l(\mathbf{x}_k)$ is the Euclidean relative distance between $\mathbf{A}^l$ and the input data vector $\mathbf{x}_k$:

$$r_l(\mathbf{x}_k) = \sqrt{\sum_{i=1}^{N} \left(a^l_{i,j_i} - x_{i,k}\right)^2} \Big/ \delta\alpha\sqrt{N} \tag{7}$$

Equation 7 defines a hyper-sphere on the input space with radius equal to $\delta\alpha\sqrt{N}$. The objective of the training algorithm is to select a subset of fuzzy subspaces as RBF centers, so that all the training data are covered by at least one hyper-sphere. Expressing this requirement in terms of Eq. 6, the subset of fuzzy subspaces is selected so that there is at least one fuzzy subspace that assigns a nonzero multidimensional degree to each input training vector.

Using more fuzzy sets for each input variable makes the grid denser and results to the selection of more RBF centers. However, the distribution of the candidate centers along the direction of each input variable is the same, as long as the same number of fuzzy sets is used for all of them. This restricts the flexibility of the algorithm, since a different partitioning for each input variable might result in a better network in terms of accuracy and/or complexity of the model. To this end, a non-symmetric variation of the algorithm was proposed [57], where the domain of each input variable i is partitioned into c_i fuzzy sets, which results to C fuzzy subspaces:

$$C = \prod_{i=1}^{N} c_i, \quad i = 1, \ldots, N \tag{8}$$

In this case, the centers and the widths of the fuzzy sets are different for each input variable and each fuzzy subspace can be represented as:

$$\mathbf{A}^l = \{\mathbf{a}^l, \boldsymbol{\delta\alpha}\} = \left\{ \left[a^l_{1,j_1}, a^l_{2,j_2}, \ldots, a^l_{N,j_N}\right], [\delta\alpha_1, \delta\alpha_2, \ldots, \delta\alpha_N] \right\}, \quad l = 1, \ldots, C \tag{9}$$

Equation 7, defining the Euclidean relative distance, should be adapted to the case of non-symmetric partition, where the hyper-sphere becomes an N-dimensional hyper-ellipse:

$$r_l(\mathbf{x}_k) = \sqrt{\sum_{i=1}^{N} \left(\left(a^l_{i,j_i} - x_{i,k}\right)^2 / N(\delta\alpha_i)^2 \right)} \tag{10}$$

The replacement of the original spherical relative distance equation with an ellipsoidal one makes the non-symmetric algorithm more flexible, as it gives the user the opportunity to partition the domain of each input variable in a different way. Thus, the resulting RBFs cover more efficiently the regions of the input space where input data are available and produce networks with higher accuracy (smaller modeling error) and/or lower complexity.

After replacing the relative distance equation, the algorithm finds the subset of fuzzy subspaces that assign a nonzero multidimensional degree to all input training vectors, proceeding in the same way with the symmetric approach. The synaptic weights are calculated using linear regression of the hidden layer outputs to the real measured outputs (target values). The regression problem can be trivially solved using linear least squares in matrix form:

$$\mathbf{W} = \mathbf{Y}^{\mathrm{T}}\mathbf{Z}\left(\mathbf{Z}^{\mathrm{T}}\mathbf{Z}\right)^{-1} \tag{11}$$

where $\mathbf{W}$, $\mathbf{Z}$, and $\mathbf{Y}$ are matrices containing the synaptic weights, hidden layer outputs, and target values, respectively.

Results and discussion

In this study, the non-symmetric fuzzy means algorithm is used to build RBF models for predicting the refractive index using as inputs experimental data. In order to demonstrate the generic nature and applicability of the neural network approach, we distinguish two cases: In the first case, the objective is to predict n for two semiconductor crystals, while in the second, the objective is to predict n for a liquid mixture.

Case I: silicon and germanium crystals

Silicon and germanium are the most important semiconductors in solid-state technologies. These materials are associated with high thermal conductivity, high optical

damage threshold, high third order nonlinearities, and a mature fabrication technology inherited by microelectronics. As a result, there exists a continuously increasing interest in silicon and germanium for photonics applications [60] ranging from infrared passive elements such as lenses and waveguides, to active components such as wavelength converters and laser amplifiers. As a result of this interest, accurate knowledge of optical constants of silicon and germanium is very important. To this end, Frey et al. [61] measured the absolute refractive index using the Cryogenetic High-Accuracy Refraction Measuring System (CHARMS) at NASA's Goddard Space Flight Center, as a function of both wavelength λ and temperature T for silicon and germanium crystals. The range of these measurements, which have all an accuracy of five decimal digits, can be found in Table 1. In the same study, the measured data were fitted to a temperature-dependent Sellmeier model.

In this article, neural network models were trained to predict the refractive index for each semiconductor crystal using as inputs the wavelength and temperature. For the case of silicon, a set of 156 input–output pairs was available, which was split into training and validation datasets. The issue of properly splitting the datasets for neural network applications has been the focus of many studies [62]. Although there is no consensus on the subject, the general practice is to allocate more data for model training. The ratio of 70–30% for training and validation datasets, respectively, is one of the most common ones found in the literature [63] and has been also adopted in this study. The data were assigned to the two datasets randomly, except for the three minimum and maximum values for each input which were kept in the training dataset. This was done to guarantee that the neural network would not extrapolate outside of the limits of training (as depicted in Table 1), where the prediction performance could deteriorate significantly. The inability to guarantee a good performance outside the limits of training is common for all black-box approaches, as these methodologies do not use a predefined form of equation, but are based solely on the available training data [64]. In order to find the optimum partition of the input space, an exhaustive search was performed testing all combinations of partitions ranging from 5 to 50 fuzzy sets for each input variable.

Table 1 Case I: measurement range for silicon and germanium

	Silicon		Germanium	
	Min	Max	Min	Max
Refractive Index	3.39437	3.54498	3.93819	4.14434
Temperature (K)	30	295	30	295
Wavelength (microns)	1.1	5.5	1.8	5.5

For comparison purposes, we also trained a different RBF network using the symmetric fuzzy means algorithm. The results were validated using two statistical pointers over the validation dataset, namely, the maximum error (Max Error) and the mean absolute relative error (MARE). The latter is calculated using the following equation:

$$\mathrm{MARE} = \frac{\sum_{k=1}^{K} \frac{|y_k - \hat{y}_k|}{y_k}}{K} \tag{12}$$

where y_k are the real measurements and $\hat{y}_k$ the neural network predictions.

Table 2 summarizes the results in the validation dataset for the two different neural networks and the Sellmeier model, depicting also the optimal number of fuzzy sets, the number of RBF centers employed by the RBF networks, and the total computational time measured on a PC with Core 2 quad processor at 2.83 GHz. It can be seen that the non-symmetric algorithm outperforms in terms of accuracy not only the symmetric approach, but more importantly the Sellmeier model which has been built solely for this purpose. The superiority of the proposed approach becomes more apparent taking into account that the Sellmeier coefficients have been fitted on exactly the same dataset used for validation of the model, while the NN models are validated on a dataset that has not been used during the training phase of the network. This obviously sets a handicap for the two neural network models, but nevertheless the non-symmetric fuzzy means algorithm outperforms the Sellmeier model. It should be noted that the symmetric approach completes the training in shorter computational times, which is expected since there are much fewer combinations of fuzzy sets to test during the exhaustive search phase. However, the non-symmetric algorithm offers increased accuracy while keeping the total

Table 2 Case I: silicon results

	Fuzzy partition		Computational time (s)	Centers	Max error	MARE
	T	λ				
RBF non-symmetric	24	34	42	69	8.58×10^{-4}	3.16×10^{-5}
RBF symmetric	31	31	11	73	8.61×10^{-4}	4.32×10^{-5}
Sellmeier equation	–	–	–	–	1.04×10^{-3}	3.20×10^{-5}

computational time in an acceptable value. Figure 3 depicts the prediction errors for the non-symmetric approach and the Sellmeier equation, while Fig. 4 shows a three-dimensional plot of the surface predicted by the RBF network trained with the non-symmetric algorithm, together with the experimentally measured data points.

Regarding the case of germanium crystals, Frey et al. [61] reported a set of 108 input–output pairs consisting of temperature–wavelength and refractive index measurements. Employing a similar process with the case of silicon, the data were assigned in training and validation datasets and then two RBF models were trained. Table 3 provides a comparison between the different approaches in the validation dataset. Once more, the RBF model trained with the non-symmetric fuzzy means algorithm proves to be more accurate in terms of smaller maximum and mean errors on a dataset independent from the one used for training. This can also be seen in Fig. 5, where the prediction errors for the non-symmetric approach and the Sellmeier equation are depicted. The surface predicted by the RBF network trained with the non-symmetric algorithm is shown in Fig. 6, together with the experimentally measured data points.

It should be noted that in both cases of silicon and germanium, the mean error of the neural network predictions is in the fifth decimal place, i.e., the prediction accuracy approximates the measurement accuracy.

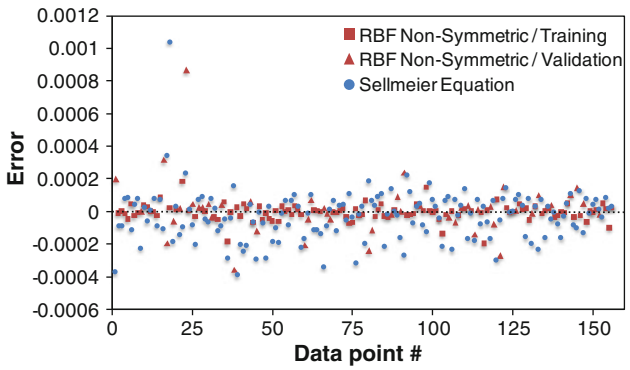

Fig. 3 Prediction errors for the RBF network trained with the non-symmetric algorithm and the Sellmeier equation for Case I: silicon crystal

Case II: ethanol–water mixture

In order to establish the application-independent nature of our approach, we have tested it in a different case, namely, the modeling of the refractive index in two-component mixtures. This problem has a twofold significance: Refractive index measurements may be used with such mixtures as a diagnostic tool for determining the relative concentration, while they are also suitable to provide physical information about the molecular evolution in the mixed systems. In [65], Jimenez-Rioboo et al. report a set of experimental refractive index data for ethanol–water solutions. This is a particularly interesting study, since it has been shown that the refractive index of an ethanol–water mixture does not follow a simple mixture rule: in fact, n shows a decrease for low water concentrations, although the refractive index of water is lower than that of ethanol [65].

In order to model this nonlinear behavior, we have trained neural networks that can predict the refractive index of an ethanol–water mixture, using as inputs the mixture concentration in water C and the temperature T. The experimental work reported in [65] consists of a set of 446 input–output data, where n is measured with an accuracy of six decimal digits. The range of these measurements can be found in Table 4. The next step was to split the data randomly to a training and validation dataset, keeping the three minimum and maximum values for each input to the

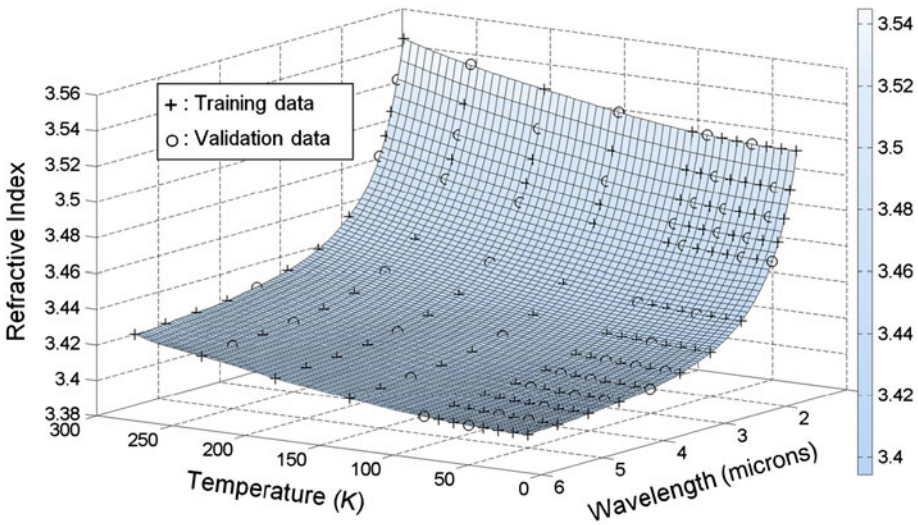

Fig. 4 Refractive index predicted by the RBF network trained with the non-symmetric algorithm for Case I: silicon crystal

Table 3 Case I: germanium results

	Fuzzy partition		Computational time (s)	Centers	Max error	MARE
	T	λ				
RBF non-symmetric	10	26	36	42	2.84×10^{-4}	2.63×10^{-5}
RBF symmetric	14	14	10	43	5.72×10^{-4}	3.26×10^{-5}
Sellmeier equation	–	–	–	–	2.10×10^{-3}	3.87×10^{-5}

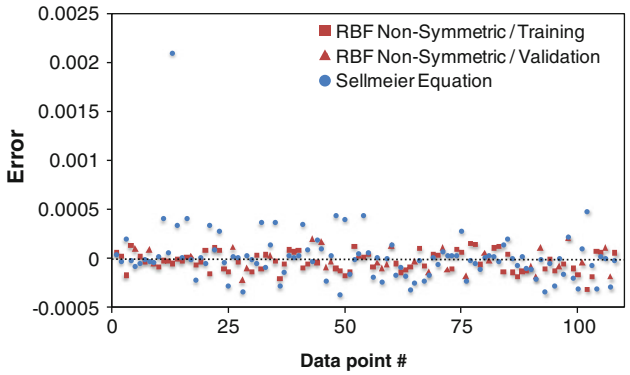

Fig. 5 Prediction errors for the RBF network trained with the non-symmetric algorithm and the Sellmeier equation for Case I: germanium crystal

training dataset. Similar to Case I, two RBF neural network models were created, trained with the non-symmetric, and the symmetric fuzzy means algorithms, respectively. Table 5 summarizes the results, where the superiority of the network trained with the non-symmetric algorithm in terms of accuracy is obvious. It can be seen that n can be approximated with an accuracy that can reach six decimal places, i.e., almost equal to the number of decimal places in the actual measurements.

It should be noted that the Sellmeier equation is not applicable in this case, and no other empirical equation for correlating the refractive index with the concentration and temperature is reported in [65]. Instead, an attempt to fit the experimental data to a second degree polynomial is presented; however, the fit is limited to a narrow range of temperatures ($15\ ^\circ\text{C} < T < 25\ ^\circ\text{C}$), whereas the neural network model provides good approximation throughout the measurement range. Figure 7 depicts the surface plot of the refractive index predicted by the RBF network trained with the non-symmetric algorithm versus the concentration and temperature, together with the experimentally measured data points.

Table 4 Case II: measurement range for ethanol–water mixture

	Min	Max
Refractive index	1.358977	1.372772
Temperature (°C)	0	27
Concentration (water mol%)	1.09	51.89

Conclusions

This study presents a new methodology for predicting the refractive index of various materials, based on experimental data. The mathematical model that correlates the refractive index with the experimental inputs is based on an

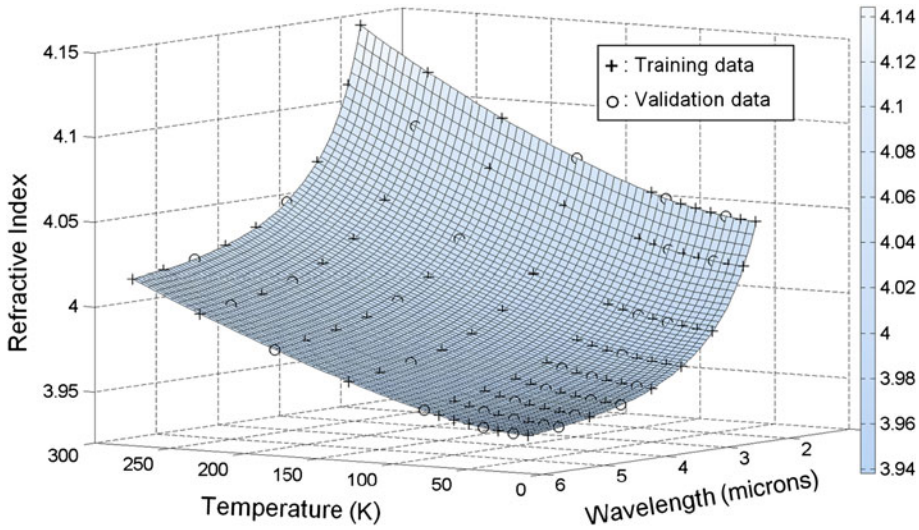

Fig. 6 Refractive index predicted by the RBF network trained with the non-symmetric algorithm for Case I: germanium crystal

Table 5 Case II: ethanol–water mixture results

	Fuzzy partition		Computational time (s)	Centers	Max error	MARE
	C	*T*				
RBF non-symmetric	48	10	84	60	3.63×10^{-5}	9.14×10^{-6}
RBF symmetric	17	17	22	62	4.08×10^{-5}	1.04×10^{-5}

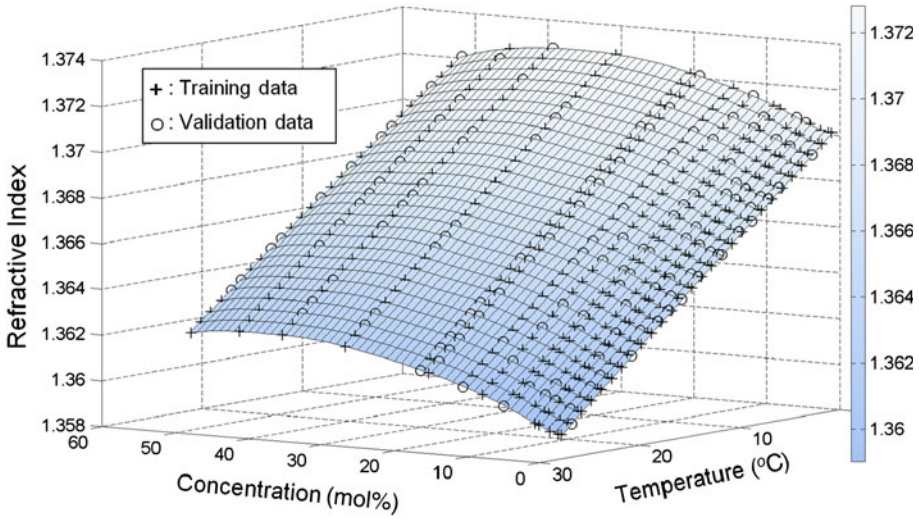

Fig. 7 Refractive index predicted by the RBF network for Case II: ethanol–water mixture

RBF neural network trained with the non-symmetric fuzzy means algorithm, which presents higher approximation accuracy compared to other training methodologies. The proposed approach was applied in cases consisting of different materials, namely, two semiconductor crystals and a binary liquid mixture, and the results showed that the produced models provide an accuracy of several decimal places that in most cases is equal to the number of decimal places in the actual measurements, while successfully taking into account various parameters affecting the refractive index. In fact, for the case of predicting the refractive index in semi-conductor crystals, the neural network approach surpassed in terms of accuracy standard methodologies used for this purpose as the Sellmeier equation. The generic nature of the neural network approach and the fact that neural networks can approximate any nonlinear function provided that sufficient training data are available, indicate that the same approach can be applied for refractive index prediction in any kind and form of material.

References

1. Hervé P, Vandamme LKJ (1994) Infrared Phys Technol 35(4): 609
2. Knoll W (1998) Annu Rev Phys Chem 49:569
3. Lisa G, Lisa C (2007) Rev Roum Chim 52:647
4. Kang E-S, Lee TH, Bae BS (2002) Appl Phys Lett 81:1438
5. Schlarb U, Betzler K (1993) J Appl Phys 73(7):3472
6. Cross M, Adams MJ (1974) Opt Quantum Electron 6(3):199
7. Souri D, Salehizadeh SA (2009) J Mater Sci 44:5800. doi: 10.1007/s10853-009-3814-z
8. Ouendadji S, Ghemid S, Bouarissa N, Meradji H, Hassan FEH (2011) J Mater Sci 46:3855. doi:10.1007/s10853-011-5306-1
9. Jlassi I, Elhouichet H, Ferid M (2011) J Mater Sci 46:806. doi: 10.1007/s10853-010-4820-x
10. Obreja P, Kusko M, Cristea D, Purica M, Comanescu F (2006) Doped polymers with controllable refractive index—preparation, processing and applications. In: Symposium on photonics technologies for 7th framework program, Wroclaw, pp 392–395
11. Böhm J, Haußelt J, Henzi P, Litfin K, Hanemann T (2004) Adv Eng Mater 6:52
12. Molla AR, Tarafder A, Karmakar B (2011) J Mater Sci 46:2967. doi:10.1007/s10853-010-5173-1
13. Austin RW, Halikas G (1976) The index of refraction of seawater. Scripps Institute of oceanography, Technical Report SIO Ref. No. 76-1
14. Harvey AH, Gallagher JS, Sengers JMHL (1998) J Phys Chem Ref Data 27(4):761
15. Ciddor PE (1996) Appl Opt 35(9):1566
16. Moosmüller H, Arnott WP (1996) Opt Lett 21:438
17. Longhurst RS (1973) General and physical optics. Longmans, London
18. Jarvis PR, Meeten GH (1986) J Phys E Sci Instrum 19:296
19. Zvirgzd JA (1975) Phys Status Solidi A 32(2):K181
20. Meeten GH (ed) (1986) Refraction and extinction of polymers. Optical properties of polymers. Elsevier Applied Science, London
21. Nussbaumer RJ, Halter M, Tervoort T, Caseri WR, Smith P (2005) J Mater Sci 40:575. doi:10.1007/s10853-005-6291-z
22. Zhang J, Lu ZH, Wang LJ (2008) Appl Opt 47(17):3143
23. Hum DS, Fejer MM (2007) Comptes Rendus Phys 8:180

24. Valdivia CE, Sones CL, Scott JG, Mailis S, Eason RW, Scrymgeour DA, Gopalan V, Jungk T, Soergel E, Clark I (2005) Appl Phys Lett 86:022906
25. Stone JA, Stejskal A (2004) Metrologia 41(3):189
26. Endo Y, Tagiri-Endo M, Seo HK, Fujimoto K (2001) J Chromatogr A 911(1):39
27. Shaw CJ, Huang A, Zhang X (2003) J Chromatogr A 987(1–2): 439
28. Tan CH, Huanga ZJ, Huang XG (2010) Anal Biochem 401(1): 144
29. Sellmeier W (1871) Ann der Phys und Chem 219:272
30. Ghosh G, Endo M, Iwasaki T (1994) J Lightwave Technol 12(8):1338
31. Liu Y, Daum PH (2008) J Aerosol Sci 39(11):974
32. Xu J, Chen B, Zhang Q, Guo B (2004) Polymer 45(26):8651
33. Rabah M, Abbar B, Al-Douri Y, Bouhafs B, Sahraoui B (2003) Mater Sci Eng B 100(2):163
34. Yu X, Yi B, Wang X (2007) J Comput Chem 28(14):2336
35. Cao X, Hancock BC, Leyva N, Becker J, Yu W, Masterson VM (2009) Int J Pharm 368(1–2):16
36. Haykin S (1999) Neural networks: a comprehensive foundation, 2nd edn. Prentice Hall, Upper Saddle River, NJ
37. Moody J, Darken C (1989) Neural Comput 2:281
38. Sarimveis H, Alexandridis A, Tsekouras G, Bafas G (2002) Ind Eng Chem Res 41:751
39. Ning L (2009) J Mater Sci 44:3156. doi:10.1007/s10853-009-3420-0
40. Lin YC, Fang X, Wang YP (2008) J Mater Sci 43:5508. doi: 10.1007/s10853-008-2832-6
41. Garcia-Mateo C, Capdevila C, Caballero FG, CGd Andres (2007) J Mater Sci 42:5391. doi:10.1007/s10853-006-0881-2
42. Mandal S, Sivaprasad PV, Dube RK (2007) J Mater Sci 42:2724. doi:10.1007/s10853-006-1275-1
43. Liujie X, Jiandong X, Shizhong W, Tao P, Yongzhen Z, Rui L (2007) J Mater Sci 42:2565. doi:10.1007/s10853-006-1278-y
44. Nazari A, Milani AA (2011) J Mater Sci 46(18):6007. doi: 10.1007/s10853-011-5563-z
45. Ejigu EK, Lacquet BM (2010) S Afr J Sci 106(7–8):56
46. Schubert MF, Poxson DJ, Mont FW, Kim JK, Schubert EF (2010) Appl Phys Express 3:082502
47. Fernandes VR, Vicente CMS, Wada N, André PS, Ferreira RAS (2010) Opt Express 18(16):16580
48. Ghosh S, Dutta PK, Bose DN (1999) Mater Sci Semicond Process 2(1):1
49. Tabet MF, McGahan WA (2000) Thin Solid Films 370(1–2):122
50. Darken C, Moody J (1990) Fast adaptive K-means clustering: some empirical results. In: IEEE INNS international joint conference on neural networks, San Diego, CA, pp 233–238
51. Afantitis A, Melagraki G, Makridima K, Alexandridis A, Sarimveis H, Iglessi-Markopoulou O (2005) J Mol Struct Theochem 716:193
52. Melagraki G, Afantitis A, Sarimveis H, Igglessi-Markopoulou O, Alexandridis A (2006) Mol Divers 10:213
53. Alexandridis A, Sarimveis H, Bafas G (2003) Neural Netw 16:1003
54. Alexandridis A, Sarimveis H (2005) AICHE J 51(9):2495
55. Alexandridis A, Patrinos P, Sarimveis H, Tsekouras G (2005) Chemom Intell Lab Syst 75:149
56. Patrinos P, Alexandridis A, Ninos K, Sarimveis H (2010) Int J Neural Syst 20(5):365
57. Alexandridis A, Sarimveis H, Ninos K (2011) Adv Eng Softw 42(10):830
58. Zadeh LA (1996) Fuzzy sets, fuzzy logic and fuzzy systems. World Scientific, River Edge, NJ
59. Nie J (1997) IEEE Trans Fuzzy Syst 5:304
60. Soref R (2010) Nat Photon 4:495
61. Frey BJ, Leviton BD, Madison TJ (2006) Temperature-dependent refractive index of silicon and germanium. In: Proceedings of the SPIE, vol 6273. SPIE, Orlando, Fla
62. May RJ, Maier HR, Dandy GC (2010) Neural Netw 23(2):283
63. Haofei Z, Guoping X, Fangting Y, Han Y (2007) Expert Syst Appl 33(2):347
64. Nelles O (2001) Nonlinear system identification: from classical approaches to neural networks and fuzzy models. Springer, Berlin
65. Jiménez Riobóo RJ, Philipp M, Ramos MA, Kruger JK (2009) Eur Phys J E 30:19